

Alma Mater Studiorum Università di Bologna  
Archivio istituzionale della ricerca

Pull-out behavior of twisted steel connectors employed in masonry: The influence of the substrate

This is the final peer-reviewed author's accepted manuscript (postprint) of the following publication:

*Published Version:*

Gentilini C., Finelli F., Girelli V.A., Franzoni E. (2021). Pull-out behavior of twisted steel connectors employed in masonry: The influence of the substrate. CONSTRUCTION AND BUILDING MATERIALS, 274, 1-14 [10.1016/j.conbuildmat.2020.122115].

*Availability:*

This version is available at: <https://hdl.handle.net/11585/806171> since: 2021-02-25

*Published:*

DOI: <http://doi.org/10.1016/j.conbuildmat.2020.122115>

*Terms of use:*

Some rights reserved. The terms and conditions for the reuse of this version of the manuscript are specified in the publishing policy. For all terms of use and more information see the publisher's website.

This item was downloaded from IRIS Università di Bologna (<https://cris.unibo.it/>).  
When citing, please refer to the published version.

(Article begins on next page)

# **Pull-out behavior of twisted steel connectors employed in masonry: the influence of the substrate**

Cristina Gentilini<sup>1a\*</sup>, Francesco Finelli<sup>2b</sup>, Valentina Alena Girelli<sup>3b</sup>, Elisa Franzoni<sup>4c</sup>

<sup>a</sup>DA – Department of Architecture, University of Bologna, Viale del Risorgimento 2, 40136 Bologna, Italy

<sup>b</sup>DICAM – Department of Civil, Chemical, Environmental and Materials Engineering, University of Bologna, Viale del Risorgimento 2, 40136 Bologna, Italy

<sup>c</sup>DICAM – Department of Civil, Chemical, Environmental and Materials Engineering, University of Bologna, Via Terracini 28, 40131 Bologna, Italy

<sup>1</sup>cristina.gentilini@unibo.it (\* corresponding author), <sup>2</sup>francesco.finelli@unibo.it,

<sup>3</sup>valentina.girelli@unibo.it, <sup>4</sup>elisa.franzoni@unibo.it

## **Highlights**

- Pull-out tests of twisted steel bars inserted in different substrates were conducted
- Bricks and stones were taken as substrates
- Both monotonic loading and two unloading/reloading cycles were applied to the steel bars
- A detailed 3D scanning of the inner surface of the hole after pull-out tests was conducted
- Results showed a clear correlation between the connector pull-out load and the compressive strength of the substrate materials.

**Keywords:** pull-out test, twisted steel bars, Neapolitan tuff, Lecce stone, fired-clay bricks, mechanical tests, abrasion resistance, masonry, connectors, 3D scanning.

## **Abstract**

It is well known that multi-leaf walls, cavity walls as well as rubble masonry are prone to brittle collapse mechanism due to weak transverse connections. Twisted steel bars are widely used to strengthen such kind of masonry buildings, in particular to improve the transverse connection between different structural elements.

Due to the shape of the twisted bar, the connector works as a self-threading screw, anchoring to the substrate material without any binder. The effectiveness of such technique mainly relies on the bond between the bar and the substrate, which relies on mechanical interlocking and friction mechanisms. In this paper, an experimental study on the pull-out behavior of twisted steel connectors inserted in units of different materials (bricks and stones) that can be commonly found in existing masonry buildings is presented. Mechanical and microstructural characterization of the substrate materials was conducted to investigate the influence of some key parameters (compressive strength, tensile

strength, elastic modulus as well as abrasion resistance) on the pull-off load of the connector. To get a preliminary insight on the structural behavior of such connectors in presence of different loading regimes, the bars were also subjected to two cycles of unloading/reloading. Additionally, a 3D scanner was employed to geometrically characterize the inner surface of the hole left by the bar after its extraction. Results showed that among the different mechanical and microstructural parameters investigated, the substrate compressive strength plays a key role in the pull-out behavior of the connectors.

## **1. INTRODUCTION**

In the past, the selection of materials to be used for the construction of buildings depended mainly on their local availability [1] rather than on their mechanical characteristics (except for outstanding structures, such as towers, city walls, etc.), and the overall performance of the walls was ensured by increasing their thickness. In locations with abundance of clay, bricks were manufactured, but the pre-industrial manufacturing process and the high variability of the firing temperature inside the kiln generally led to bricks having a great heterogeneity [2] and, frequently, also low mechanical performances. However, when clay was not available for bricks manufacturing, stones were used, including also soft stones such as volcanic tuff and porous limestone. It is well known that both brick and masonry buildings are not earthquake-resistant structures, due to several reasons such as the poor mechanical strength of the constituent materials and the weak connection among bricks or stone blocks due to the lack of mortar in some cases (dry masonry) or to the use of low-strength mortars. Additionally, multi-leaf walls, veneer masonry walls, cavity walls and rubble-stone masonry are characterized by weak transverse connections that may lead to out-of-plane delamination of external masonry leaves in case of seismic action [3-7]. In order to overcome these problems, strengthening techniques are often necessary to improve the transversal bond between the wall leaves and to ensure a monolithic behavior of the structure. In case of multi-leaf walls, there are several available techniques to improve transverse connections and hinder the delamination of masonry leaves. The most widespread solution consists on the injections of cement-based or lime-based grouts inside the wall, aiming at filling the voids and so improving the weakness of the internal core, and also connecting it to the external leaves [8]. A mechanically efficient alternative to grout injections is the insertion of tie bars (also named connectors) throughout the entire thickness of the wall [9], to improve the connection among the leaves, in particular between the external ones, and to reduce the transversal deformation. Connectors can be different for type and material, the most common being rigid FRP bars with carbon, glass or basalt fibers [10, 11]. FRP connectors are usually inserted in holes drilled in the substrate and then a grout is injected to fill the

hole as well as the surrounding voids and cracks [9, 12]. FRP anchor spikes are also available in the market. They are strands of bundle fibers of carbon or glass which are restrained inside a fabric sheath and are inserted into concrete or masonry substrate, fixing them by epoxy resin. The free end of the anchor spike is fanned-out and fixed by epoxy resin to the surface [13]. Recently, a connector system constituted by a stainless treaded steel rod inserted in a fabric sleeve was introduced, which is inserted in a hole drilled in the wall and then pressure-injected with high-strength cement-based grout [14, 15]. A recent study carried out on the shear behavior of multi-leaf masonry specimens with several types of transversal connectors pointed out the lack of literature on this topic and the need of experimentations for extending the available dataset [16]. Other studies highlighted that the out-of-plane behavior of connectors received limited attention in literature, hence further research is needed for a better insight on their actual effectiveness [17].

Besides the above described connectors, a new type of connector was recently proposed, which consists in a twisted high-strength steel bar and is characterized by a high ease of application and installation [18]. In this case, bars are inserted in masonry walls by means of a special mandrel, exploiting a pre-drilled hole whose diameter is slightly smaller than the nominal diameter of the connector. Such procedure is expected to ensure a good mechanical interlocking between the bar and the substrate material, without any need of binder (resin or grout) [18]. The dry application allows to save time and money in the strengthening intervention and avoids the possible compatibility issues related to the use of resins or cement-based grouts, and these aspects have contributed to the diffusion of helical-shaped connectors. At the surface of the walls, the bars are anchored just folding the protruding part on the masonry surface with a hammer. Alternatively, plastic circular plugs can be screwed at the head of the bar and fixed injecting a small quantity of resin. In other cases, dry-inserted connectors are used to connect textile-reinforced renders applied over the two faces of the masonry [19].

Although these connectors are made available in the market by several manufacturers and are commonly used in buildings, only very few studies have been carried out about their mechanical behavior and their effectiveness as retrofitting method [18, 20, 21]. The pull-out behavior of helical stainless-steel bars inserted in a single type of lime-based mortar substrate was investigated in [18], taking into account several parameters, i.e. bar diameter, pre-drilled hole diameter and anchorage length. Results showed that bond strength increased for tight pre-drilled holes but decreased for the greatest bar diameter, while good correlations were found between bond strength and anchorage length. In another study, helical steel bars, dry inserted within the masonry to connect the two textile-reinforced mortar layers, led to crack localization, with no significant improvement on the

post-cracking behavior, highlighting how urgent is achieving a better knowledge of the connectors behavior and actual effectiveness [19].

In the present paper, the bond behavior between of twisted steel bars inserted in different substrate materials was investigated. The interlocking was considered a crucial parameter to study, as without an adequate interlocking, the connector cannot act efficiently and its application could result ineffective [19]. On the other hand, the performance of any kind of anchor is strongly affected by the parent masonry material properties [17], hence this aspect was considered for the present experimental campaign. Investigating the behavior of connectors in different materials is particularly important also in the light of the variety of substrates that can be found in historic buildings, ranging from fired-clay bricks (very heterogeneous) to several stones exhibiting dramatically different characteristics.

Within this context, the present research aims at analyzing the pull-out response of twisted connectors inserted in different substrates, for a better understanding of the mechanical interaction between bar and substrate. Five kinds of materials typically used in existing constructions were considered, namely three types of fired-clay bricks and two natural stones, i.e. Neapolitan tuff and Lecce stone. Mechanical properties such as compression, splitting tensile strength and elastic modulus were determined. Additionally, the substrate material properties such as abrasion resistance, bulk density and porosity were determined in order to investigate their role on the bar pull-out response. After insertion of the connectors in the substrates, the bars were subjected to two different loading schemes: monotonic tensile loading up to failure and tensile loading with two unloading-reloading cycles before increasing the load up to failure.

After the pull-out tests, the bar was completely extracted by the substrate, which was then longitudinally cut into two halves. In order to geometrically characterize in details the inner surface of the hole left by the bar after pull-out, 3D scanning technique was employed, using a structured-light projection scanner and analyzing the 3D model obtained. It is well known that lasers and 3D scanners are today considered among the most reliable, efficient and accurate tools for objects measuring. Thanks to the technological improvements in electronics and sensors, nowadays the available accuracy has promoted the use of these instruments in a wide range of applications: Cultural Heritage documentation also for restoration purposes [22], archaeology, mechanical and civil engineering [23], medicine, gaming, entertainment industry [24], etc. For those applications requiring very high accuracy, triangulating lasers or 3D scanners are usually chosen. In certain applications, the availability of an extremely detailed high-precision 3D model permits the accurate study of the surface geometric characteristics, as for example the roughness of road pavements [25], or the geometrical characterization of Wire-and-Arc Additive Manufactured stainless steel elements

[26]. In addition, thanks to the application of digital filters and artificial light to the model, the three-dimensionality of the surface can be opportunely emphasized, helping for example the interpretation of engravings and inscriptions in archaeological finds [27].

## 2. MATERIALS AND METHODS

### 2.1. Materials

The most commonly used twisted connectors are characterized by a diameter equal to 10 mm, although 12 mm bars have been recently introduced in the market as well. In the present study, the 10 mm connectors were selected for the experimental campaign. A single size was selected, as the aim of the study was to investigate the role of different substrate materials, rather than the influence of the geometry of the connectors. The connectors are made of high-strength stainless steel (AISI 316) and exhibit nominal diameter,  $\phi_{BAR}$  (defined as the diameter of the circle that circumscribes the cross-section of the bar), and cross-sectional area,  $A_{BAR}$ , equal to 10 mm and 14.5 mm<sup>2</sup>, respectively, Fig. 1a. The bars were formed by cold working starting from a circular steel wire. The distance between the ribs is equal to 30 mm.

For the insertion of the steel connectors, 250 × 120 × 55 mm<sup>3</sup> blocks of different materials were used. In particular, three types of solid fired-clay bricks were tested and two types of natural stones, so as to consider a range of natural and artificial materials characteristic of historic buildings and exhibiting different mechanical and microstructural properties.

The fired-clay bricks used are two types of solid red bricks (labelled as SM and RB) and a yellow one (labelled as YB). Based on the technical data sheets provided by the manufacturers, all the bricks were shaped by pressure, in order to reproduce the features of ancient bricks, hence they belong to the class of so-called “handmade bricks”. In particular, YB contains rough inclusions in the original clay mix, like the pre-industrial bricks commonly found in many historic buildings [28]. The natural stones used are Neapolitan tuff stone and Lecce stone, labelled as NT and LS, respectively. Neapolitan tuff is the building material mostly used in historic architecture in Naples (Italy). This material is a macroporous rock of volcanic origin containing different amount of pumice, zeolites, analcime and feldspar [29]. Lecce stone is a pale yellow, bioclastic limestone from the Salento area (Southern Italy), extracted mainly from the quarries near the city of Lecce, from which this stone takes its name. This stone was used in the past as the main building material of Baroque monumental structures giving the characteristic cream color to many cities in this region [30]. It is a soft, microporous stone, with high total porosity; it is mainly composed of calcite, with traces of phosphatic minerals and quartz. NT and LS stones were cut in blocks having the same dimensions of the bricks, i.e. 250 × 120 × 55 mm<sup>3</sup>.



Fig. 1. a) Twisted bar and b) original cross-section of the bar before twisting (size in mm).

## 2.2. Materials characterization

### 2.2.1. Characterization of steel connectors

In order to assess the mechanical properties of the steel connectors, direct tensile tests were performed. An anchorage system consisting of aluminium pipes filled with a thixotropic bi-component epoxy resin was employed, Fig. 2a. The specimens, having a total length of 800 mm, were provided with two 150 mm long anchoring elements (external diameter 11 mm, internal diameter 8 mm), resulting in a free length equal to 500 mm [31]. A universal testing machine was used for the tests, with maximum capacity of 600 kN. Each specimen was provided with a clip-on-gauge (length equal to 100 mm) placed in the central position of the bar to record the elongation, Fig. 2b, and the load was applied at a constant speed of 2 mm/min until the failure of the specimen (Fig. 2c). A total of three bars were tested.

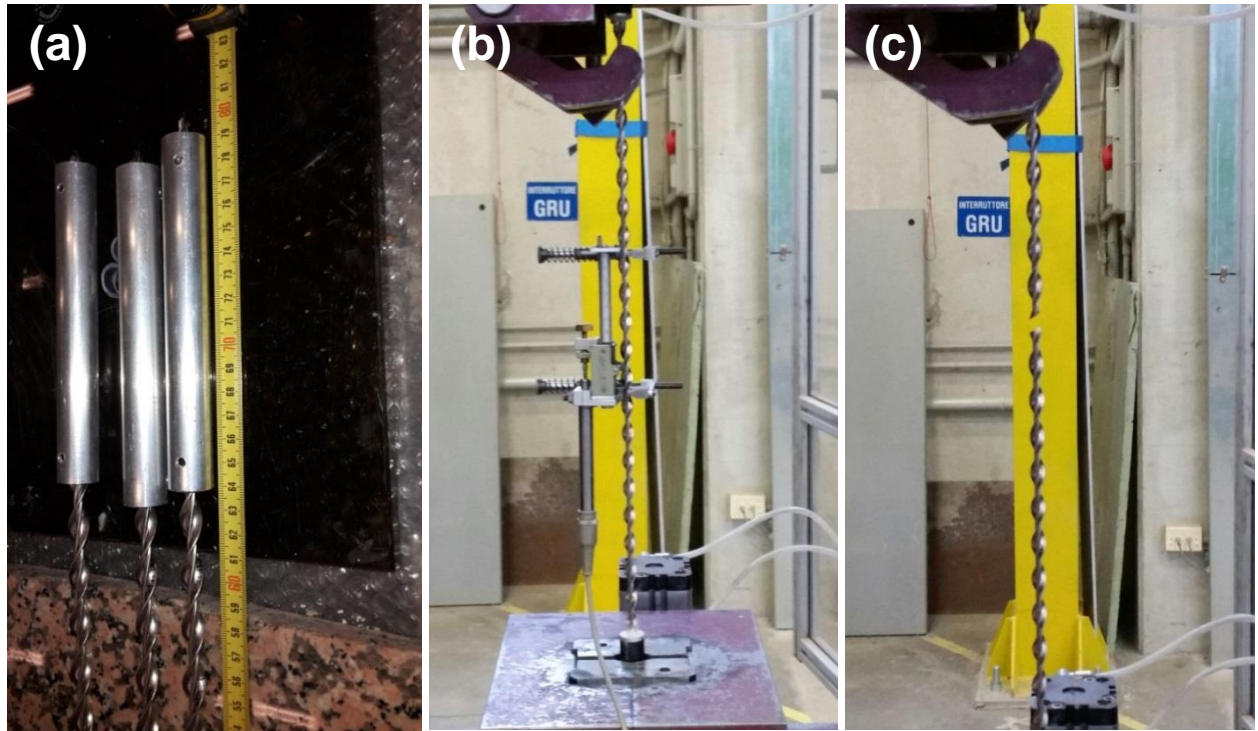


Fig. 2. Tensile testing of the steel connectors: a) detail of the aluminum pipes employed as anchorage system; b) a steel connector during the test with the clip gauge placed in the central position; c) a steel connector after failure.

### 2.2.2. Characterization of bricks and stones

The mechanical properties of the fired-clay bricks and stones were obtained experimentally. The following parameters were determined: Young's modulus ( $E$ ), compressive strength ( $f_c$ ), indirect tensile strength ( $f_t$ ), and abrasion resistance.

Five cylindrical samples (diameter 50 mm and height 50 mm) were core-drilled from each material. One of the five cylinders was subjected to a monotonic axial compressive loading in a universal testing machine with maximum capacity of 100 kN, applying the load at a rate equal to 0.2 MPa/s, according to EN 772-1 [32], in order to determine its compressive strength, whose value is required for the following determination of the Young's modulus. It worth noting that six specimens are required in EN 772-1 for the determination of compressive strength, while in the present study five specimens per type were used. However, the results shown further on (Table 2) highlight that the standard deviation among specimens of the same material was quite limited, hence testing an additional specimen was not expected to change significantly the average value obtained for the compressive strength. Young's modulus was obtained on the remaining four cylinders of each series, according to the procedure in EN 14580 [33], except for the fact that the height to diameter ratio for the determination of the elastic modulus was 1 in this study, rather than 2 (ration indicated in the standard). The reason for this choice was that compressive strength and elastic modulus were



both measured perpendicularly to the bricks and stone units, i.e. in the same direction used in the materials' datasheets in the market. Although a small overestimation of this Young's modulus can be expected using a height to diameter ratio equal to 1 (due to some confining effect of the bearing plates), this aspect is not expected to particularly influence the interpretation of the results for the aim of the present study. The specimens were provided with two vertical strain gauges symmetrically displayed in the central position with respect to the height of the cylinders, Fig. 3a. The loading procedure provided that the specimens were subjected to three loading-unloading cycles in the range 2% - 33% of the expected maximum load, with a loading rate equal to 0.5 MPa/s. Once the last loading cycle was performed, the specimens were loaded monotonically up to failure, Fig. 3b. The elastic modulus is the slope of the last loading branch, calculated as the ratio between the stress difference and the corresponding strain difference. In this way,  $f_c$  was averaged on 5 samples and  $E$  on 4 samples.

Indirect tensile strength was determined according to Brazilian splitting test, EN 12390 [34]. Four cylinders for each series were tested, at a loading rate equal to 0.05 MPa/s. In Fig. 4a, a Neapolitan tuff specimen is shown before testing, while in Fig. 4b the load-displacement curves obtained for all the NT cylinders are reported. Compression and indirect tensile tests were not performed on SM samples, since mechanical data for this batch of bricks were already available from a previous study [35].

The abrasion resistance of the bricks and stones was determined on prismatic samples ( $55 \times 55 \times 10$  mm<sup>3</sup>), in terms of weight loss after an accelerated abrasion test, based on a modified version of the Porcelain Enamel Institute (PEI) abrasion test, developed by the authors [36]. Briefly, the modified test consists in keeping the sample in a rotary motion, at a constant speed (300 rpm), against an abrasive mixture constituted by 57.7 g of steel balls (having different diameters between 1 and 5 mm) and 1.0 g of corundum grit (80 mesh) for a pre-fixed revolution number (7500). The abraded area is circular and has a radius of 47 mm. The abrasion resistance of the material is expressed, after blowing the surface with compressed air, as its weight loss per unit surface area. The bulk density and open porosity of the materials were determined by water saturation at room pressure and hydrostatic weighing.

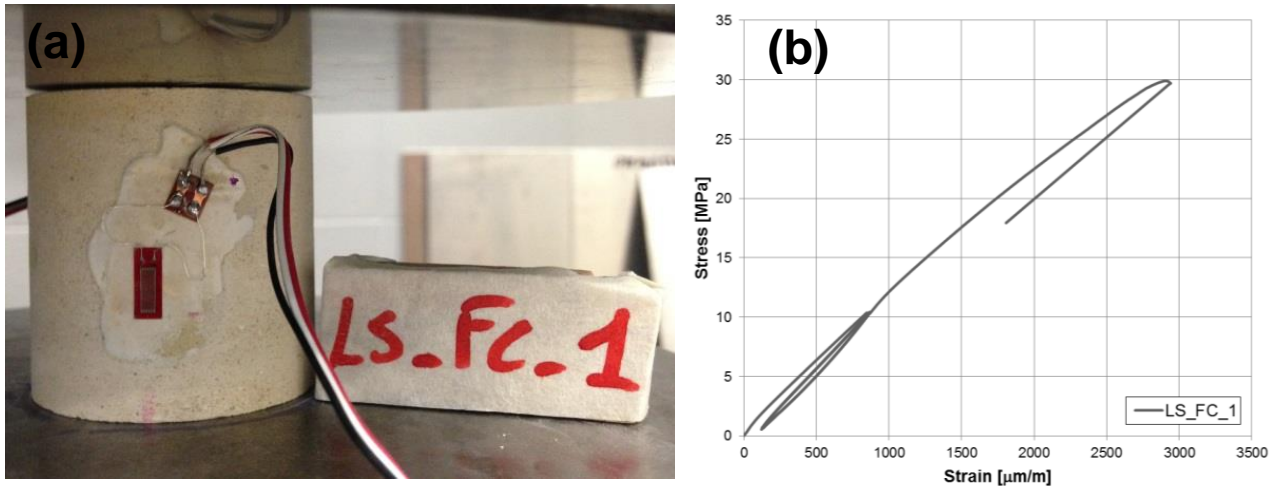


Fig. 3. Compression test on the substrate materials: a) a representative Lecce stone specimen before testing; b) its stress-strain curve.

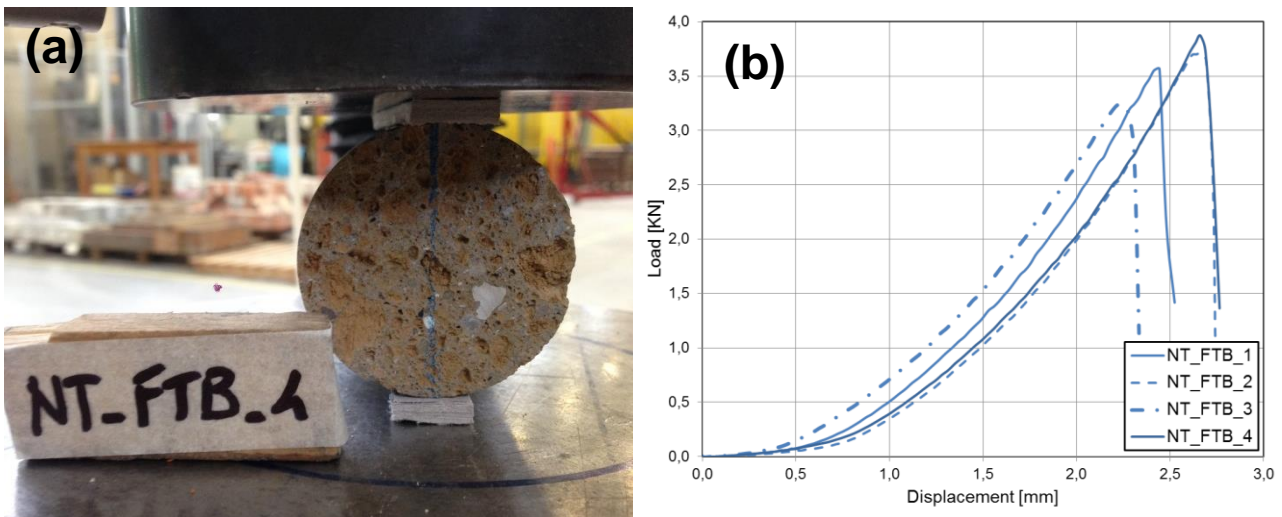


Fig. 4. Brazilian test on the substrate materials: a) a representative Neapolitan tuff specimen before testing; and b) load-displacement curves for all the NT specimens.

## 2.3. Pull-out test and 3D scanning

### 2.3.1. Preparation of the specimens: insertion of the connectors

Following the procedure described in the manufacturer's data sheet [37], a pilot hole was drilled in the central position of each block, in the longitudinal direction (length 250 mm). It should be noted that when the bars are employed in the field to improve the connections between the leaves of a masonry wall, they are inserted crossing the bricks in the width direction (120 mm direction in this study). However, the depth of insertion is usually at least twice this length, since the connector crosses two or more bricks depending on the leaves number. For this reason, in this study the bar was inserted in the longest direction (250 mm), in order to consider this scenario.

The drill tip that was employed for the holes had a nominal diameter equal to 8 mm. Once the holes were drilled, a 450 mm long steel connector was inserted in each brick by percussion using the mandrel provided by the manufacturer. During the insertion, the bar rotated into the pilot hole as a screw due to its shape, producing some visible powdering of the substrate in the hole. Because of the material indentation during insertion, the final diameter of the hole is expected to be slightly larger than the initial one. After the insertion, the bars protruded out for a length of about 100 mm from both sides of the samples, as in Fig. 5. Five specimens per substrate material were prepared.

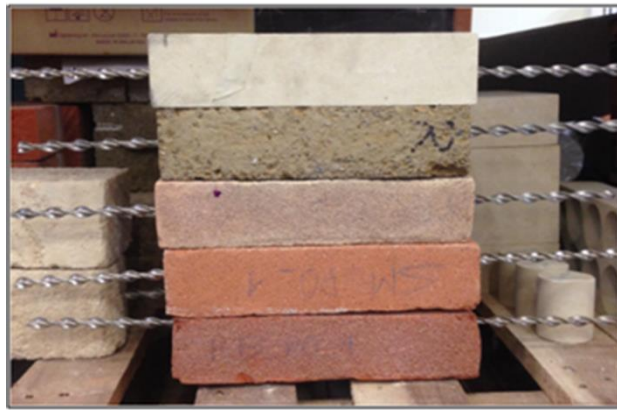


Fig. 5. Specimens with the connectors before the pull-out test. From top to bottom: LS, NT, YB, SM, RB.

### ***2.3.2. Pull-out test set-up and procedure***

A total of 25 pull-out tests were performed, according to the test set-up shown in Fig. 6. The pull-out force was applied by a universal testing machine of maximum capacity 100 kN. The top end of the bar (1 in Fig. 6), for a length equal to 50 mm, was directly grabbed by the head of the machine with an edge shaped grip. It should be noted that two different methods of grabbing the bars were employed: aluminum pipes at the ends of the bar in case of tensile tests and direct grabbing of the bar ends with the machine grips in the pull-out tests. In the case of tensile tests, the bar was subjected to a tensile force up to failure, hence it was necessary to adopt an anchoring system that led to a correct failure mode of the bars in correspondence of the center. In the case of pull-out test, since the expected maximum loads are lower than the ultimate load of the bar, the use of a grabbing system was not necessary. The reaction to the pull-out load was provided by a bearing steel plate with a circular hole of 48 mm diameter (3 in Fig. 6). Due to the twisted shape of the bar, it tends to rotate during the test and hence to drag the brick in which it is inserted. Thus, the rotation of the loaded end of the connector and that of the brick around the vertical axis were prevented. The first was avoided by locking the rotation of the machine head and the second was blocked with a steel grip in contact with an edge of the brick and fixed to the top plate (2 in Fig. 6).

The top slip was monitored by the displacement of the head of the machine, while the bottom slip was measured by two 50 mm linear variable displacement transducers, LVDTs (4 in Fig. 6). The tips of the transducers, fixed to the bearing plate by means of magnets, reacted off of an aluminum circular-shaped plate connected to the unloaded end of the bar (6 in Fig. 6). The average of these two displacements measured by the two LVDTs is named ‘bottom slip’ in the following of the paper. The ‘top slip’ is the displacement measured by the machine head. In fact, the elastic deformation of the free part of the bar, i.e. the protruding part between the brick top surface and the machine grip (which was just 2-3), was considered negligible.

Tests were performed in monotonic mode and displacement control with a rate of 0.05 mm/s. It should be noted that one specimen of each series was subjected to two unloading and reloading cycles, in order to obtain preliminary information about the mechanical behavior of the connectors in presence of cyclic actions. There was no load inversion, since the connectors were not suitable to withstand significant compression actions.

In Table 1, the labels of the specimens and the testing modes are summarized.

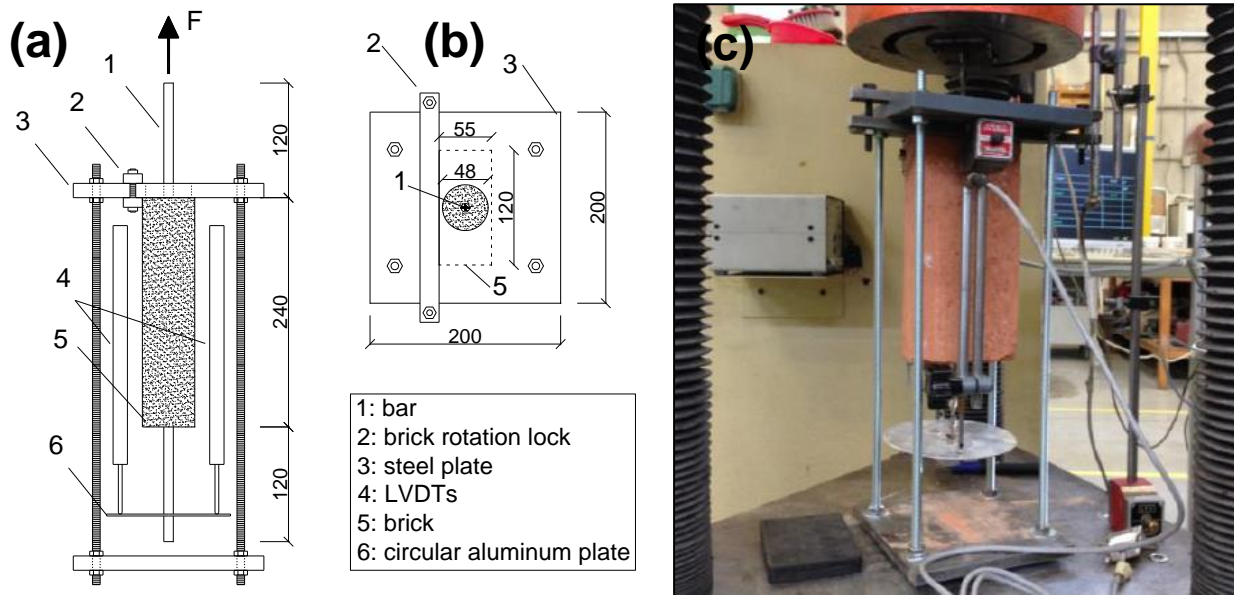


Fig. 6. Pull-out test set-up (sizes in mm): a) lateral view; b) top view and c) a specimen (SM series) at the beginning of the test.

Table 1. Specimens for the pull-out tests.

Substrate material	Specimen label	Testing mode
Solid fired-clay brick	SM_PO_1	Monotonic loading
	SM_PO_2	

SM	SM_PO_3	Two unloading and reloading cycles
	SM_PO_4	
	SM_PO_C	
Solid fired-clay brick YB	YB_PO_1	Monotonic loading
	YB_PO_2	
	YB_PO_3	
	YB_PO_4	
	YB_PO_C	Two unloading and reloading cycles
Solid fired-clay brick RB	RB_PO_1	Monotonic loading
	RB_PO_2	
	RB_PO_3	
	RB_PO_4	
	RB_PO_C	Two unloading and reloading cycles
Neapolitan tuff NT	NT_PO_1	Monotonic loading
	NT_PO_2	
	NT_PO_3	
	NT_PO_4	
	NT_PO_C	Two unloading and reloading cycles
Lecce stone LS	LS_PO_1	Monotonic loading
	LS_PO_2	
	LS_PO_3	
	LS_PO_4	
	LS_PO_C	Two unloading and reloading cycles

### 2.3.3. 3D scanning of the hole surface after pull-out tests

After pull-out, a specimen per type for a total of 5 specimens, was selected for the 3D scanning, in order to geometrically characterize the surface of the hole left by the bar. The 3D scanning of the hole is expected to provide additional information on the failure mechanism of the bar-substrate system and on the effectiveness of the connectors in anchoring to the substrates. In fact, the high-precision 3D scanning may allow to detect the presence, pitch and depth of the grooves left by the bar ribs and hence to help the interpretation of the pull-out test results. To this aim, the bar was completely extracted from the block, which afterwards was longitudinally cut with a circular saw. A high-resolution 3D scanning of the cut surface was performed, using a structured-light projection

scanner Artec Spider, Fig. 7. This instrument operates substantially by the classic topographic triangulation principle: a regular pattern of light is projected on the object, which consequently appears distorted due to the surface shape. A sensor inside the instrument is able to elaborate the distortion for the 3D mesh reconstruction of the surface geometry. This scanner combines high speed and accuracy: 1 million points acquired with an accuracy of 50 microns. About 4 million triangles with an average edge length of 0.1 mm constituted all the five obtained 3D models. For each specimen, the best-fit cylinder of the hole was derived. This is the ideal cylinder that best fits the surface that is the one that minimizes the deviations between mesh and cylinder, where deviations are the geometric differences between the two 3D models. The deviations between the mesh of the hole and the best-fit cylinder were analysed using a colour map visualization and extracting some statistical parameters, as the variance and average values of deviations (both positive and negative values were calculated). A positive average value ( $Avg^+$ ) of the deviations is obtained in those parts where the mesh of the hole is above the best-fit cylinder, that is, it protrudes compared to the cylinder; vice versa a negative average value ( $Avg^-$ ) refers to those parts where the mesh is below the cylinder.

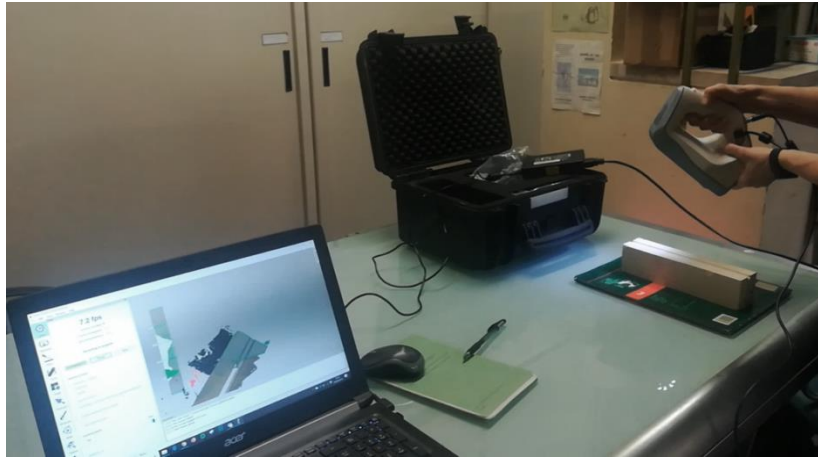


Figure 7. Portable instrument during the high-resolution 3D scanning of the hole surface of a specimen.

### 3. RESULTS AND DISCUSSION

#### 3.1. Materials characterization

##### 3.1.1. Characterization of steel connectors

Average tensile strength  $f_{t,BAR}$ , elastic modulus  $E_{BAR}$ , and breaking elongation  $\epsilon_{BAR}$  of the connectors after the tensile tests result equal to 1109 MPa (CoV=0.7%), 134 GPa (CoV=9.2%) and 3.62% (CoV=11.8%), respectively, in line with what is expected for this kind of materials.

### 3.1.2. Characterization of bricks and stones

Results obtained for all the materials are collected as average values in Table 2.

Lecce stone exhibits the highest compressive and tensile strength values, as well as a much higher Young's modulus (13.7 GPa) compared to the other materials, whose  $E$  ranges between 3 and 7 GPa. As any natural stone, Lecce stone can be characterized by a wide spectrum of performances, depending on the specific location and quarry of extraction, and the investigated stone can be classified as a high quality one according to [38]. The two red bricks, SM and RB, exhibit mechanical characteristics and porosity values that are typical for this kind of materials, and can be considered representative of ordinary bricks. The yellow brick (YB) shows a high porosity (44.5%) and low mechanical performance, being its compressive strength less than one third compared to the other two bricks. The presence of visible inclusions and grains in the original clay mix are responsible for the scattering observed in the results. Neapolitan tuff (NT) exhibits low mechanical performance, as expected on the basis of its volcanic origin and presence of ash, and very low bulk density (1277 kg/m<sup>3</sup>). However, the open porosity of NT is comparable with those of SM and RB, which may appear as a contradiction, but it must be noticed that a high number of closed pores are surely present in the tuff due to its volcanic origin and these cannot be detected through water absorption test, so the value of total porosity probably exceeds the open porosity value reported in Table 2. Based on these results, NT and YB can be considered representative of porous, weak and soft masonry materials, RB and SM are representative of bricks of ordinary quality and LS is representative of a high-quality natural stone.

In terms of abrasion loss, the results are more difficult to interpret and to correlate to the other properties in Table 2, also due to the high coefficients of variation. In LS, NT and YB, the high scattering is ascribed to the presence of inclusions and macro-grains in the materials [36]: micro-fossils in Lecce stone, ash inclusions in tuff and nodules in the original clay of yellow brick, as previously pointed out. In particular, the limited abrasion loss experienced by YB is not supported by the low quality of this material and seems related to accidental factors due to the heterogeneous nature of the original clay mix, hence a higher number of samples would be necessary.

Based on these results, the substrate materials selected in this study exhibit a wide range of mechanical and physical properties and can be considered representative of the different masonry materials that can be found in historic buildings.

Table 2. Results of mechanical characterization tests of the substrate materials (coefficients of variation in brackets).



Substrate material	Compression strength, $f_c$ [MPa]	Young's modulus, $E$ [GPa]	Tensile strength, $f_t$ [MPa]	Bulk density [kg/m <sup>3</sup> ]	Open porosity [%]	Abrasion loss [mg/cm <sup>2</sup> ]
Lecce stone (LS)	30.8 (2.8%)	13.7 (9.8%)	3.27 (15.2%)	1746 (0.4%)	24.2 (1.7%)	9.7 (45%)
Neapolitan tuff (NT)	3.9 (19.2%)	5.3 (25.5%)	0.79 (7.5%)	1277 (1.1%)	31.9 (2.5%)	15.0 (22%)
Fired-clay brick (RB)	25.8 (8.5%)	6.0 (15.8%)	2.98 (1.7%)	1731 (0.2%)	29.7 (1.5%)	17.7 (23%)
Fired-clay brick (SM)	20.3 <sup>(*)</sup>	7.3 <sup>(*)</sup>	3.16 <sup>(*)</sup>	1639 (0.5%)	33.4 (0.0%)	14.5 (2%)
Fired-clay brick (YB)	7.6 (21.7%)	3.0 (13.5%)	1.87 (31.4%)	1358 (0.5%)	44.5 (0.1%)	9.7 (26%)

<sup>(\*)</sup> value from [35]

### 3.2. Pull-out tests and 3D scanning

#### 3.3.1. Pull-out tests with monotonic loading

The load - top and load - bottom slip curves of the specimens are reported in Fig. 8a and Fig. 8b, respectively, while the pull-out test results are collected in Table 3. Notably, the curves related to the same substrate are in good agreement, a meaningful scatter existing only for NT series, probably due to the coarse inclusions and large voids that characterize this material, leading to a dispersion also in the results of the mechanical tests (Table 2). All the specimens failed for bar pull-out.



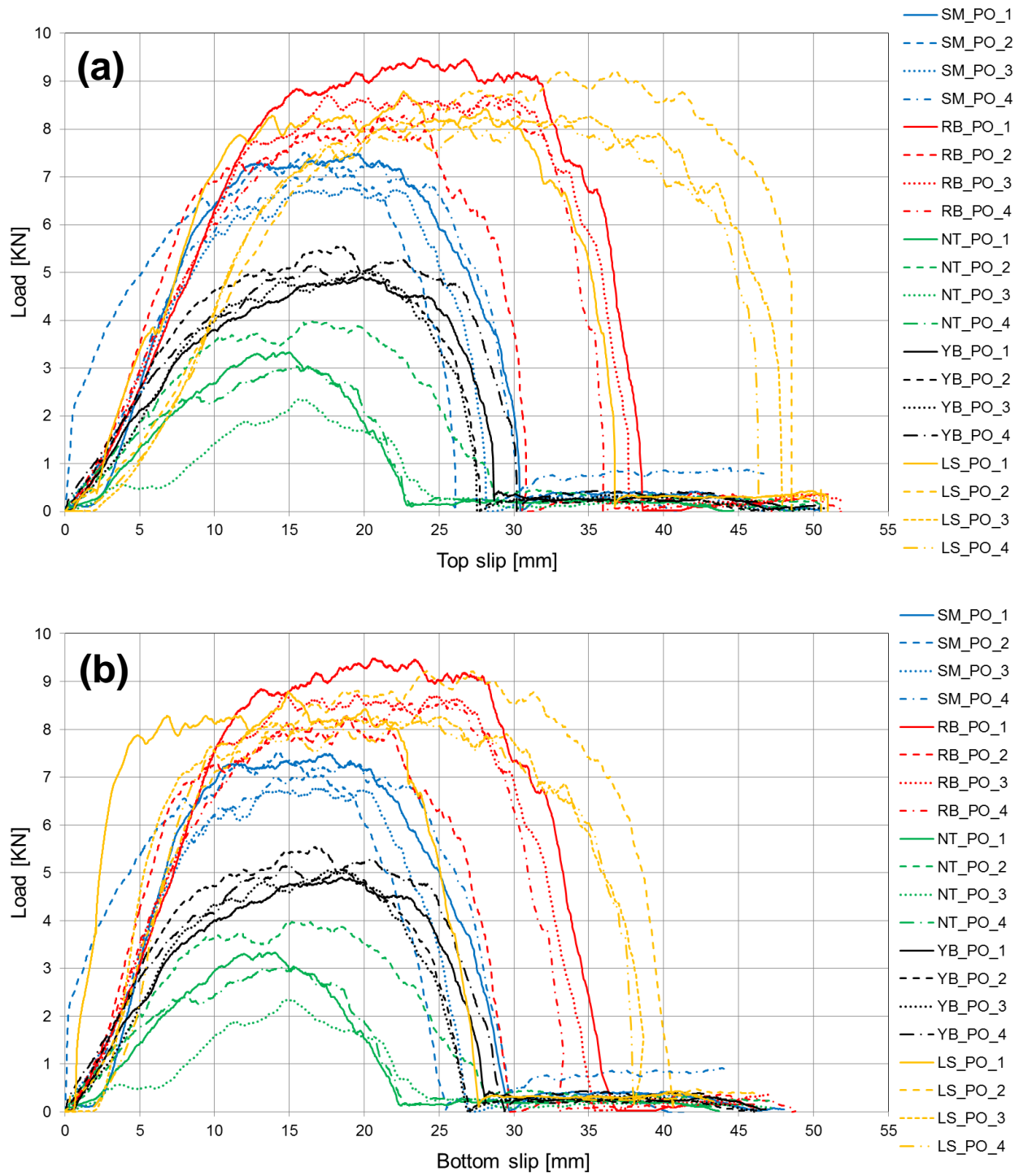


Fig. 8. a) Load - top slip curves and b) load - bottom slip curves for all the specimens.

Table 3. Pull-out test results (coefficient of variation in brackets).

Substrate material	Specimen label	Maximum Load [kN]	Average Maximum Load [kN]	Average $\Delta\text{slip}_{\text{ascending}}$ [mm]	Average $\Delta\text{slip}_{\text{descending}}$ [mm]
Solid fired-clay	SM_PO_1	7.49	7.29 (4.1%)	0.62 (26.4%)	1.74 (20.5%)
	SM_PO_2	7.54			

SM series	SM_PO_3	6.78			
	SM_PO_4	7.29			
	SM_PO_C	7.37			
Solid fired-clay RB series	RB_PO_1	9.49	8.63 (6.3%)	0.91 (11.9%)	3.06 (21.8%)
	RB_PO_2	8.28			
	RB_PO_3	8.73			
	RB_PO_4	8.57			
	RB_PO_C	8.07			
Solid fired-clay YB series	YB_PO_1	4.90	5.22 (4.9%)	0.62 (8.5%)	1.48 (16.8%)
	YB_PO_2	5.54			
	YB_PO_3	5.04			
	YB_PO_4	5.28			
	YB_PO_C	5.36			
Neapolitan tuff NT series	NT_PO_1	3.33	3.21 (18.5%)	0.41 (22.8%)	0.80 (11.8%)
	NT_PO_2	3.97			
	NT_PO_3	2.34			
	NT_PO_4	3.04			
	NT_PO_C	3.37			
Lecce stone LS series	LS_PO_1	8.79	8.58 (4.9%)	4.49 (22.2%)	11.04 (17.4%)
	LS_PO_2	9.22			
	LS_PO_3	8.28			
	LS_PO_4	8.17			
	LS_PO_C	8.47			

Referring to the LS curves in Fig. 8a and in Fig. 8b, four main parts can be clearly distinguished: *i*) a first quasi-linear ascending branch; *ii*) a plateau, in which the load is basically constant; *iii*) a third branch in which the load sharply decreases; and *iv*) a last branch where the load attains values close to zero for increasing displacements. During the pull-out test, due to its geometrical shape the bar is under a combined stress state of torsion and tension behaving like a big screw. For a better interpretation of the curves in Fig. 8, the average difference between top and bottom slip values was calculated at half of the average peak value, both in the ascending branch ( $\Delta\text{slip}_{\text{ascending}}$ ) and in the descending branch ( $\Delta\text{slip}_{\text{descending}}$ ), and the results are reported in Table 3. From the very beginning, the bottom slip registers values different from zero, and also the top slip. The substrate that is in

contact with the ribs of the bar opposes with friction, compression and shear resistance to this rotation and vertical slip. It is noteworthy that a difference was found between the bar top and the bottom slip, the latter being smaller. For LS specimens, the top slip in the ascending branch resulted equal to 7.5 mm on average, while the bottom slip was equal at the same load level to 3 mm on average, resulting in a  $\Delta\text{slip}_{\text{ascending}} \approx 4.5$  mm. This difference is thought to be related to the following effect. During loading, the bar tended to move in the hole by unscrewing, thanks to the furrow that the bar produced when it was inserted in the substrate. However, the bar head was locked to the machine, opposing to the unscrewing, so the bar also untwisted and non-uniformly elongated. In fact, even if the bar head was locked to the machine and the brick was locked as well to prevent its rotation, the free end of the connector rotated during the extraction: this torsion was visible as the circular aluminum plate rigidly connected to the free end of the bar rotated during the test, as shown in Fig. 9. This rotation increased regularly during the ascending branch (comparison between (a) and (b) in Fig. 9), but as soon as the load reached the plateau in Fig. 8, the rotation basically stopped corresponding to an increase in the displacement. Finally, when the load drop occurred, the reversible torsional strain was suddenly released and the free end of the bar rotated back (Fig. 9c), although not exactly up to the original position highlighting a residual plastic deformation. This behavior may help in the interpretation of the curves in Fig. 8. In the initial quasi-linear branch, the bar was in tension and due to its twisted shape tended to unscrew towards the bar top, which is locked to the machine, requiring an increasing load, as the substrate opposed to the unscrewing of the bar, hence causing some unscrewing of the bar. During this translation and rotation, the material substrate in between the bar lugs started to locally crush and the load reached a plateau that is higher and longer when the substrate is more mechanically resistant. When the substrate offered no more resistance to the bar slip/rotation, a sharp drop was registered in the load and the elastic part of torsional deformation was suddenly released, as confirmed by the back rotation of the free end of the bar (Fig. 9c). At this point the bar simply slipped in the substrate and the residual resistance to extraction was exclusively due to the friction between the outer surface of the ribs and the substrate, corresponding to the horizontal branch close to zero in the last part of the curves.

Notably, for all the specimens, the slip difference between the bar top and bottom increased in the descending branch being  $\Delta\text{slip}_{\text{descending}} > \Delta\text{slip}_{\text{ascending}}$  in Table 3. This suggests, as highlighted before, a non-uniform untwisting and elongation of bar.

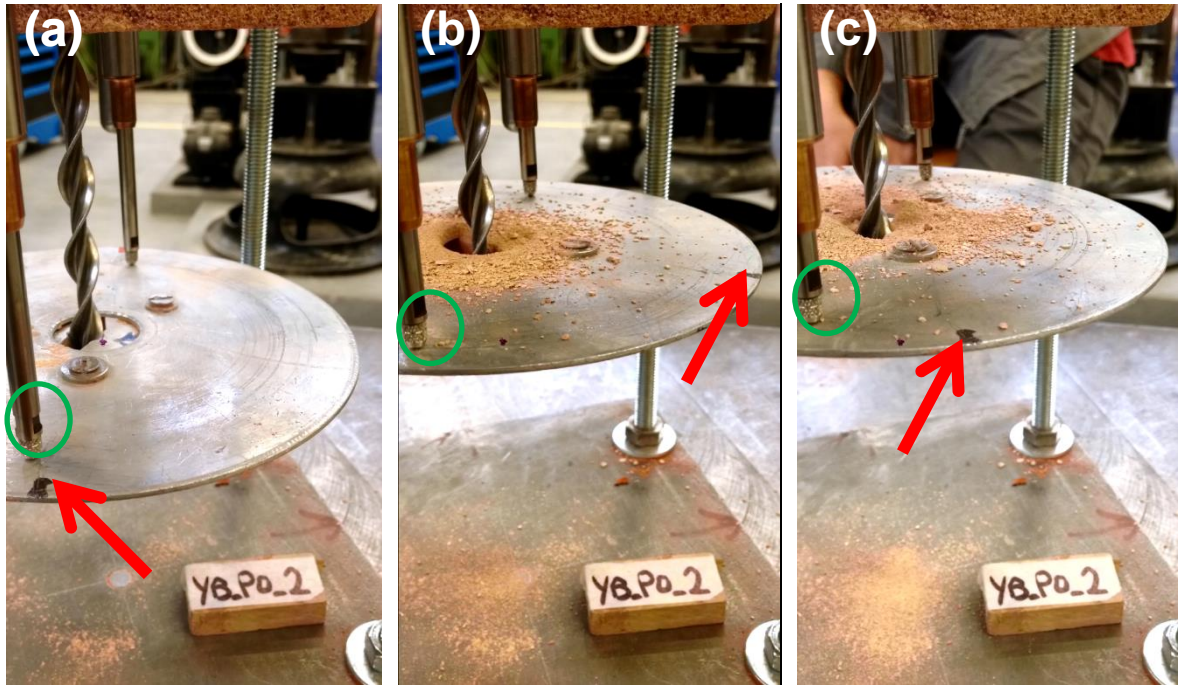


Fig. 9. Pictures taken during the test of a representative specimen of the yellow brick series (YB\_PO\_2). Detail of the free end of the connector: a) at the beginning of the test, when the LVDT tip (in the green circle) is in correspondence of the black dash (red arrow); b) during the test, when the bar rotates counterclockwise and c) at the end of the test, when the bar rotates back, towards the initial position.

Red brick (RB) substrate, characterized by high mechanical properties, exhibited a comparable behavior to LS and similar average maximum load, Fig. 8 and Table 3. However, the slip differences in the ascending and descending branch in Table 3 were smaller with respect to those of LS substrate. This is due to the higher compressive strength of LS with respect to RB ( $\sim +20\%$  in Table 2) and also to its more than double stiffness (13.7 GPa for LS rather than 6.0 GPa for RB, being the shear modulus not specifically measured). As a consequence, the rotation/slipping of the bar along the hole in LS was hindered by a more resistant material, facilitating an untwisting of the bar towards the top and resulting in a high difference between the top and bottom registered slips. Conversely, RB exhibits weaker mechanical properties than LS, hence the slip differences between top and bottom slips were smaller.

SM bricks exhibited a behavior similar to the previous two substrates, but with a lower maximum load and a smaller difference between top and bottom slips, consistently with the lower compressive strength and stiffness of this substrate.

YB and NT specimens showed the lowest maximum loads and the smallest slip difference at both ascending and descending branch, which is in line with their weaker and softer nature with respect

to the other materials. These two substrates also exhibited a not clearly visible plateau branch, which may be ascribed to the fact that the torsion of the bar was not completely hindered by these substrates, which started to pulverize from the very beginning of the bar slipping, especially in the zone close to the loaded end. In fact, the difference between top and bottom slips was very limited in both cases.

Analyzing the curves in Fig. 8 and the data in Table 3, it can be seen that the pull-out strength increases following the order  $NT < YB < SM < LS < RB$  (being the difference between LS and RB within the dispersion of the results), i.e. following the order of increasing compressive strength of the substrates. This can be better observed in the histograms of Fig. 10, where the mechanical parameters ( $f_c$ ,  $E$  and  $f_t$ ) of the materials and the pull-out loads ( $P_{pull-out}$ ) normalized with respect to the values of the NT series ( $f_{c,NT}$ ,  $E_{NT}$ ,  $f_{t,NT}$  and  $P_{pull-out,NT}$ ) are reported and compared. From this comparison, a clear correlation can be found between the pull-out load and the compressive strength of the materials. The material with the lowest compression strength is also the material with the lowest pull-out strength, and the same applies for the other substrates. It is clear that the compression strength plays a crucial role in the extraction of the bar, as the material in between the bar lugs during extraction is subjected to compression and shear. Additionally, from the weakest to the strongest material, the pull-out curves exhibit not only increasing maximum loads, but also larger and larger displacements at which the load drop occurred. In other words, the area under the curves increases. This is a very important aspect, as the area under the curves is correlated to the energy necessary for the bar extraction, so if the load drop is attained at higher slip/load values, more energy will be necessary to overcome the resistance to extraction for these materials. Interestingly, the last almost horizontal branch, in which the resistance to pull-out is just given only by friction, for all the substrate materials is basically overlapping.

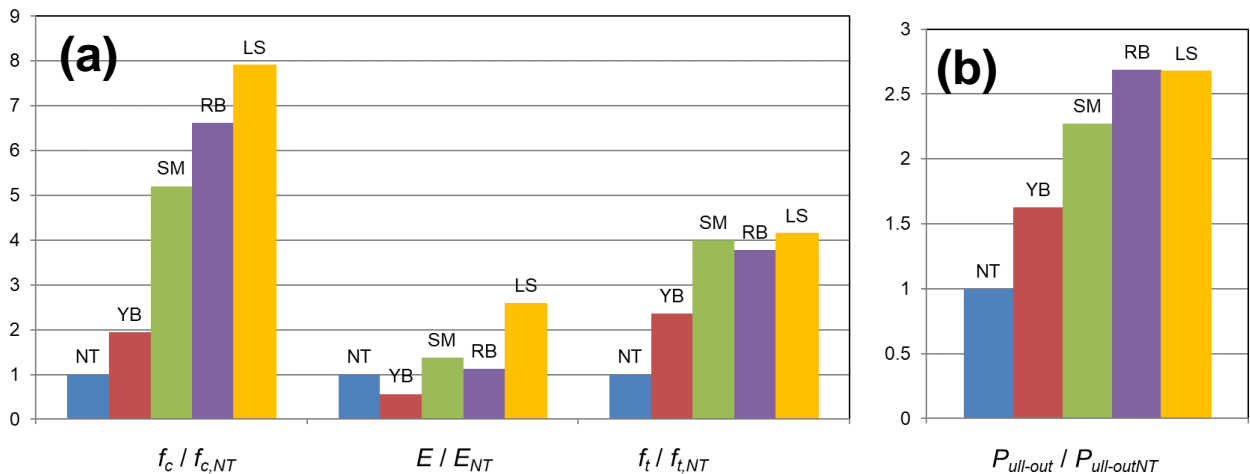


Fig. 10. Histograms of the: a) non-dimensional mechanical properties and b) non-dimensional pull-out loads for the different substrates with respect to those of Neapolitan tuff.

### ***3.3.2. Pull-out tests with unloading and reloading cycles***

In Fig. 11a and Fig. 11b, the load - top and load - bottom slip curves of the specimens that underwent two unloading and reloading cycles are collected, respectively. The first unloading was performed at a load level equal to 50% of the expected pull-out load, and the second at 75%. Specimens were unloaded till the 10% of the average maximum load registered in the monotonic tests. The aim of considering such load pattern was to estimate its influence on the load bearing capacity of the connector, to get a preliminary insight on the bar performance in case of unloading and reloading cycles. A different behavior maybe observed when larger number of cycles are considered. Therefore, it should be noted that additional tests are necessary to mechanically characterize the bar behavior in presence of seismic actions, considering tensile-compression cyclic tests with a high number of repetitions.

Results are reported in Table 3, where it can be seen that the maximum load values of these specimens are consistent with the results of the monotonic tests. Both in the first and in the second cycle, when the load level reaches the level at which the unloading cycle has begun, the loading path is recovered and no modification on the load is registered, meaning that no degradation of pull-out strength due to the cyclic loadings is recorded. It should be noted that the unloading paths are almost perfectly vertical, highlighting an irreversible deformation of the bar and substrate as noticed in the monotonic tests due to the residual torsional strain and local crushing of the material substrate. As for the monotonic tests, all the specimens, except the NT one, exhibit a plateau section after the initial quasi-linear branch, followed by a sharp load decrease and final horizontal branch where the residual resistance to slip is given only by friction.

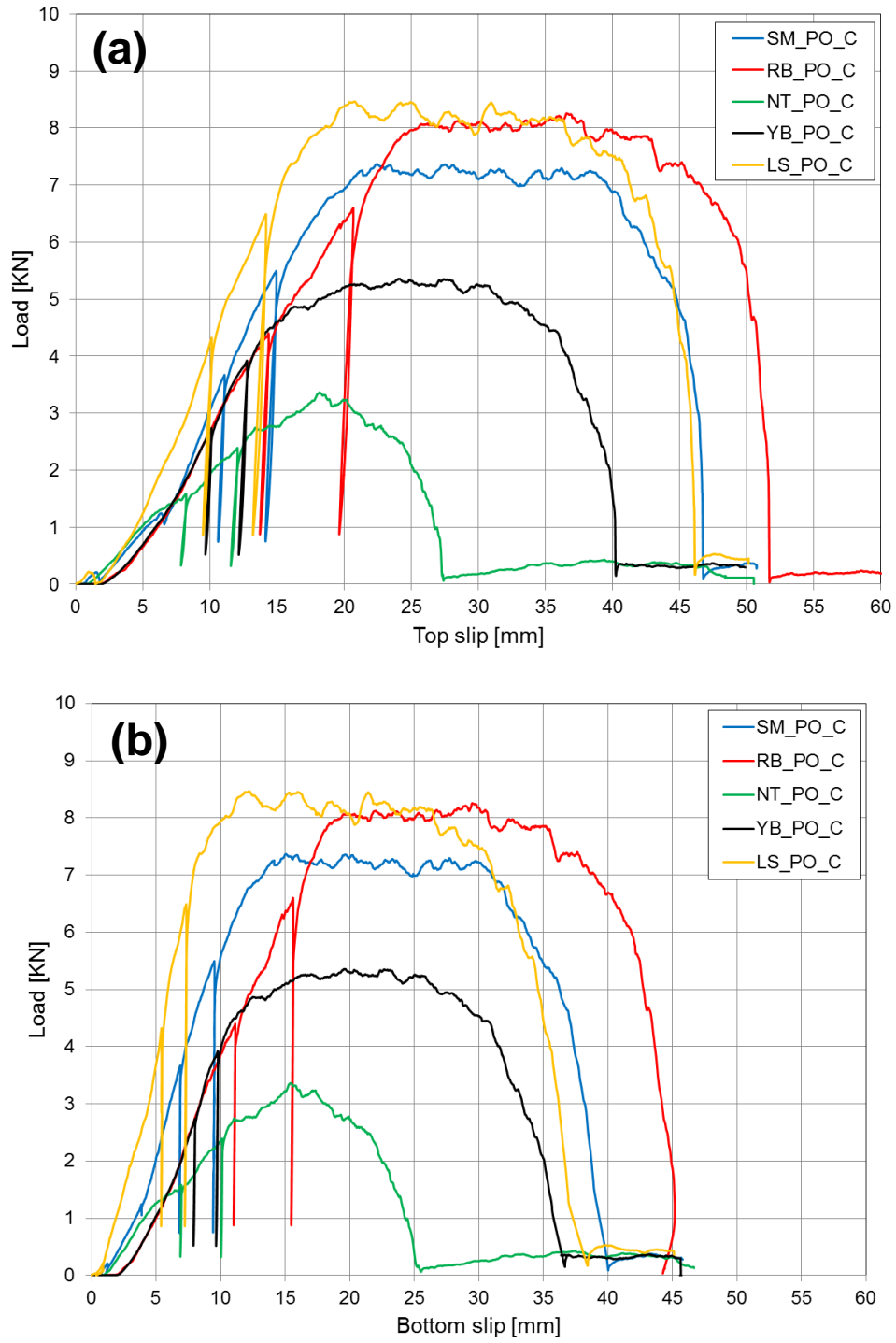


Fig. 11. a) Load-top slip curves and b) load-bottom slip curves for all the specimens which underwent two unloading and reloading cycles.

### 3.3.3. 3D scanning

The geometric characterization of the holes was made extracting the ideal cylinder that best fitted the surface and measuring the deviations between the ideal 3D cylinder and the real hole mesh. The diameters of the best-fit cylinders are reported in Table 4 together with the variance (Var), the

average positive and negative values of the deviations ( $Avg^+$  and  $Avg^-$ , respectively). In Fig. 12, the results obtained in terms of photo-textured 3D model, mesh in false colours and a portion of the mesh with the best-fit cylinder (represented in blue) are shown. It should be noted that the differences among the ideal cylinder diameters in the five substrates in Table 4 are limited, so these diameters can be considered basically comparable. The  $Avg^+$  values, which may provide an indication about the depth of embedding of the ribs of the bar during its insertion (screwing) in the blocks, confirm that the penetration of the ribs in soft materials (YB and NT) is higher than in hard ones (especially LS), as expected. However, this deeper embedding in soft materials did not provide any additional pull-out resistance, as the low compressive strength of these materials was easily overcome during the bar extraction.

In Fig. 13, the color maps of the deviations between the best-fit cylinder and the real 3D mesh hole are reported. Observing the color map of LS specimen, the imprints left by the ribs of the bar are clearly visible in diagonal (inclined light blue lines): the imprints are narrow and well defined, and this confirms that the substrate favored the unscrewing of the bar during loading, thanks to its high strength and stiffness. It also possible to observe that the distance between the ribs imprint is larger close to the loaded end (on the left in Fig. 13), confirming that the bar underwent a detorsion (unscrewing) near the locked end. The color map also highlights that the hole of LS specimen is extremely regular, thanks to the fine-grained microstructure of this stone. The two bricks RB and SM exhibit the imprint of the bar ribs, although less defined and irregular with respect to LS. Concerning YB and NT, the hole surface is characterized by large and irregular grooves indicated by the cold (blue and light blue) colors in the figure. The irregular nature of the hole surface (high  $Avg^-$  absolute values and large Var values in Table 4) are ascribed to the heterogeneity of these materials, hence the low pull-out load found for these substrates can be ascribed not only to their low mechanical performance but also to the fact that the contact between the ribs of the bar and the substrate was probably not so effective as in more homogeneous specimens.

Table 4. Geometrical parameters obtained by 3D scanning of the hole surface after pull-out tests.

Specimen	Diameter (mm)	$Avg^+$ (mm)	$Avg^-$ (mm)	Var (mm <sup>2</sup> )
SM_PO_5	9.90	0.13	-0.11	0.07
YB_PO_2	9.85	0.20	-0.41	0.34
RB_PO_5	10.02	0.17	-0.28	0.12
NT_PO_2	9.90	0.28	-0.30	0.24
LS_PO_5	10.05	0.04	-0.09	0.01




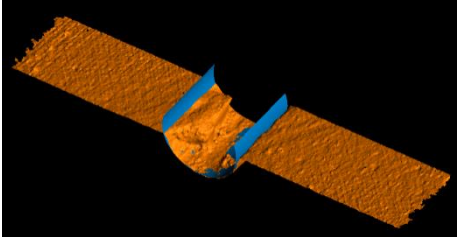

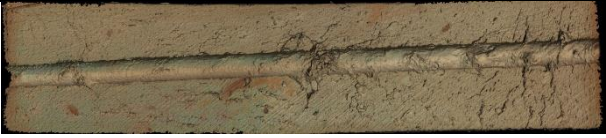
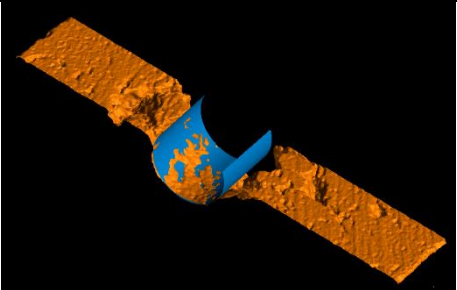
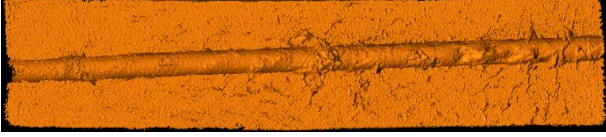

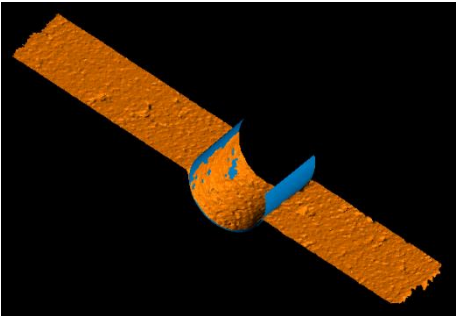


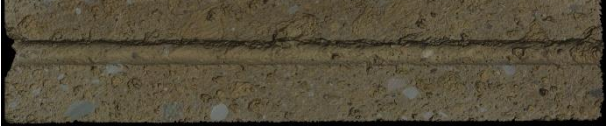
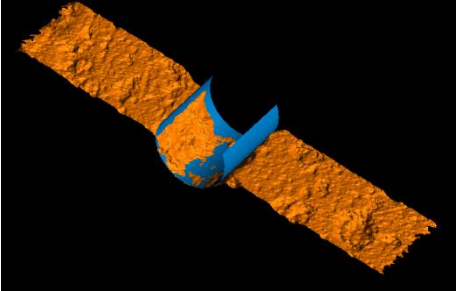


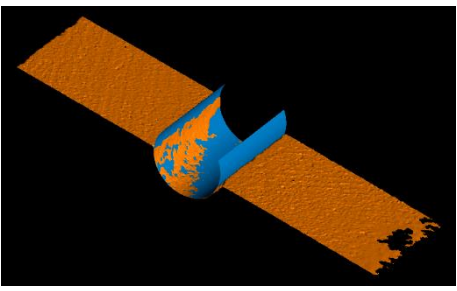
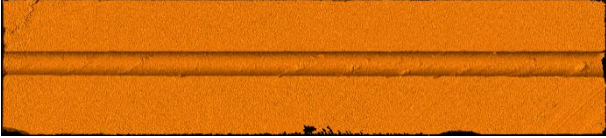
Specimen	Photo-textured 3D model (above) and mesh in false colour (below)	View clip of the mesh and, in blue, the best-fit cylinder
SM_PO_5		
		
YB_PO_2		
		
RB_PO_5		
		
		
NT_PO_2		
		
LS_PO_5		
		

Fig. 12. Results of the 3D scanning analysis of the specimens.



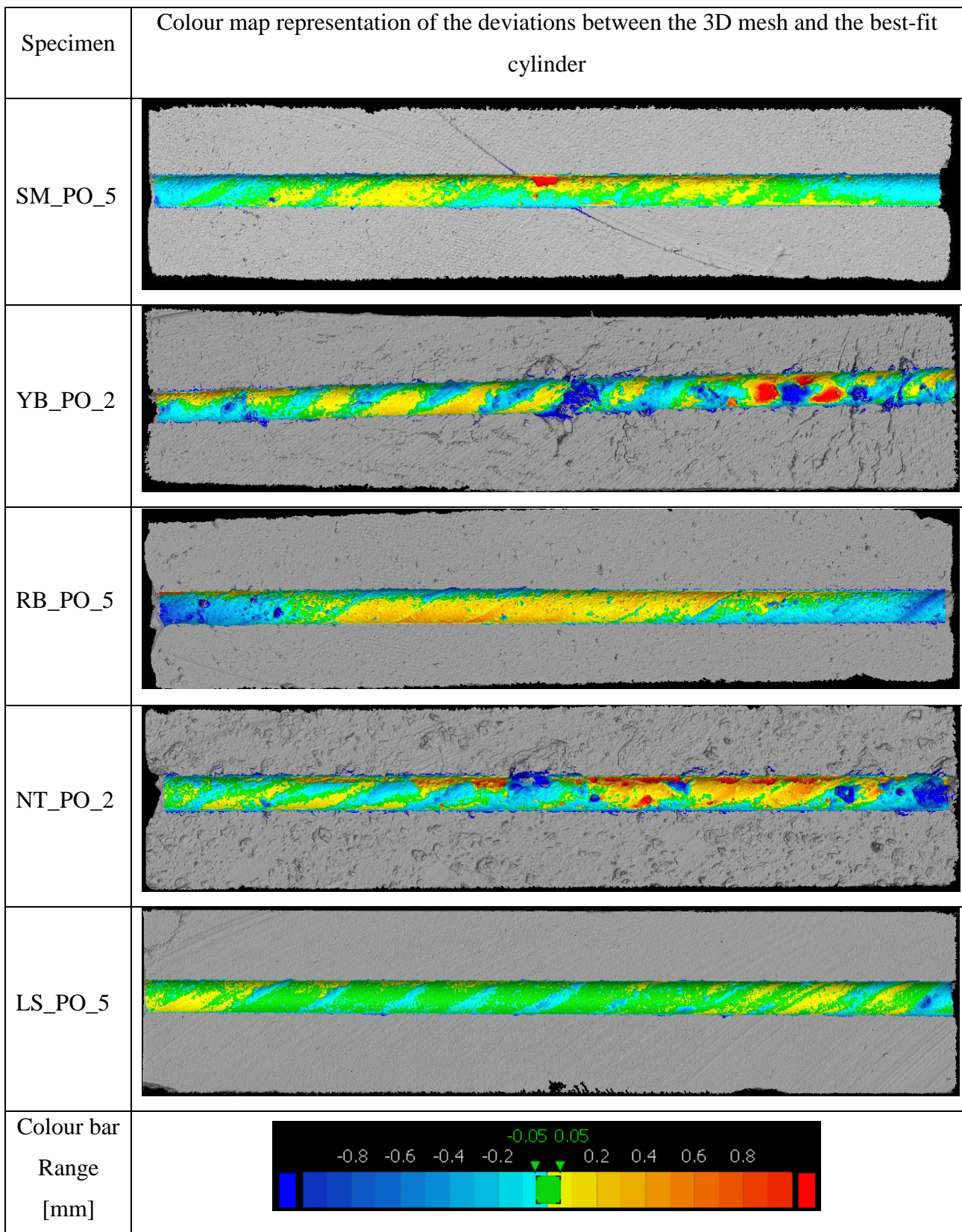


Fig. 13. Deviations between the 3D mesh of the hole and the best-fit cylinder (positive values, in warm colours, represent points inside the cylinder and negative values, in cold colours, represent points outside it).

#### 4. CONCLUSIONS

A preliminary experimental campaign on pull-out behavior of twisted steel connectors in different masonry construction materials was carried out in order to analyze the bond characteristics of such bars inserted in different substrates. The substrates selected for this study, namely three different kinds of bricks and two stones (Neapolitan tuff and Lecce stone), resulted different in terms of mechanical and microstructural features, thus providing a significant range of materials representative of those commonly employed in historic buildings. From the experimental results, the following considerations can be drawn:

- although the local stress distribution in the substrate owing to the bar extraction is a complex combination of compression and shear, the pull-out maximum load was found to be clearly correlated to the compressive strength of the material (an also to stiffness, although in a less clear way), namely increasing with increasing compressive strength. Conversely, the abrasion resistance of the substrate materials was not found to play a key role in the pull-out behavior;
- the pull-out curves of the bars exhibited different shapes according to the nature of the substrate. In strong and stiff substrates, a first quasi-linear ascending branch, a plateau, a descending branch and a final near-zero horizontal branch were found, while in weak and soft substrates the plateau was almost absent. This is an important aspect, showing that the pull-out of the bars in strong substrates involves not only a higher maximum load, but also a higher energy that must be spent during the slip of the bar, which may be a positive feature in seismic events;
- the slip of the bar in the pull-out test was ascribed to a complex combination of unscrewing, untwisting and sliding, whose interpretation was supported by the survey of the hole after the bar extraction by 3D scanning. By allowing to detect the presence, pitch and depth of the grooves left by the bar ribs, 3D scanning provided a helpful insight for the interpretation of the curves obtained in the pull-out tests. This survey confirmed a certain untwisting of the bar in strongest substrates. It also showed that the ribs of the bar more deeply penetrated in soft materials during its insertion (screwing), but this did not provide any particular mechanical benefit during the extraction of the bar. The heterogeneity of the substrate was also shown to play a role, causing an uneven contact between the bar and the material;
- the unloading/reloading cycles that were performed did not result in a degradation of the pull-out strength of the bars.

The results suggest that different levels of effectiveness can be expected in strengthening interventions when dealing with variable masonry characteristics and specific design provisions should be adopted.

The present results are expected to contribute to the enrichment of the knowledge on dry-inserted helical connectors. In fact, the use of these connectors is popular for multi-leaf walls, cavity walls and rubble-stone masonry due to the ease of application and good compatibility with the substrate, but they have been investigated in a very limited number of literature papers so far. Further parameters need to be investigated, including the geometry of the bars and anchoring system, and behavior of the connectors in small-scale masonry specimens, including the mortar joints and the presence of multi-leaves. In fact, it is important to recognize that the bond performance is influenced by several parameters (such as bar diameter, embedment length, loading regime, etc.), thus further research will be necessary to expand the available data and the knowledge on this topic. Moreover, given the complexity of the stress-strain behavior of twisted steel bars dry-inserted in porous building materials, the modeling of such behavior could be a valuable support in this field of research and will be the object of a future study. The validation of the results obtained through modeling can be made exploiting the pull-out test designed for this study, possibly modified to take into account also different loading conditions, and also using the information provided by the 3D scanning of the hole produced by the bar extraction. Some preliminary attempts were done to model the bond behavior of twisted steel bars in a single type of brick, with encouraging results in [21], but further improvements seem necessary to encompass different substrates and additional parameters.

## **Acknowledgements**

The experimental work discussed in this paper was conducted at the University of Bologna. Technicians of the laboratory LISG (Laboratory of Structural and Geotechnical Engineering) and LASTM (Laboratory of Materials Science and Technology) are gratefully acknowledged for their help during the preparation of the specimens and the execution of the tests. The authors would like to express their appreciation to Kerakoll S.p.A. (Sassuolo, Italy) for providing the composite materials. Mr. G. Sansone and Mr. P. Chen are gratefully acknowledged for their support during the experimental campaign.

## **References**

- [1] Sandrolini, F., Franzoni, E., Varum, H., Nakonieczny, R. Materials and technologies in Art Nouveau architecture: Façade decoration cases in Italy, Portugal and Poland for a consistent restoration. *Informes de la construction* (2011) 63: 5-11.
- [2] Sandrolini, F., Franzoni, E. An operative protocol for reliable measurements of moisture in porous materials of ancient buildings. *Building and Environment* (2006) 41:1372–1380
- [3] Martins, A., Vasconcelos, G., Costa, A. Experimental assessment of the mechanical behaviour of ties on brick veneers anchored to brick masonry infills. *Construction and Building Materials* (2017) 156: 515–531.
- [4] Giaretton, M., Dizhur, D., da Porto, F., Ingham, J.M. Seismic assessment and improvement of unreinforced stone masonry buildings: literature review and application to New Zealand. *Bulletin of the New Zealand Society for Earthquake Engineering* (2016) 49:148–174.
- [5] Giaretton, M., Valluzzi, M.R., Mazzon, N., Modena, C. Out-of-plane shake-table tests of strengthened multi-leaf stone masonry walls. *Bulletin of Earthquake Engineering* (2017) 15: 4299-4317.
- [6] Masia, M.J. Masonry façades in Australia and challenges for engineering research and design. In *Brick and Block Masonry - From Historical to Sustainable Masonry* – Kubica, Kwiecień & Bednarz (eds) © 2020 Taylor & Francis Group, London, ISBN 978-0-367-56586-2.
- [7] Muhit, I.B., Stewart, M.G., Masia, M.J. Experimental evaluation and probabilistic analysis of the masonry veneer wall tie characteristics. In *Brick and Block Masonry - From Historical to Sustainable Masonry* – Kubica, Kwiecień & Bednarz (eds) © 2020 Taylor & Francis Group, London, ISBN 978-0-367-56586-2.
- [8] Mauro, A., De Felice, G. Seismic assessment of multi-leaf masonry strengthen with injections or transversal ties. In *Structural Analysis of Historical Constructions* – Jerzy Jasieńko (ed) 2012 DWE, Wrocław, Poland, ISSN 0860-2395, ISBN 978-83-7125-216-7, (2012) 1873-1879.
- [9] Oliveira, D.V., Silva, R.A., Garbin, E., Lourenco, P. Strengthening of three-leaf stone masonry walls: an experimental research. *Materials and Structures* (2012) 45: 1259-1276.
- [10] Anania, L., Badalà, A. The use of carbon fiber cementitious matrix connection for the strengthening of multiple-leaves masonry. *Key Engineering Materials* (2017) 747: 366-373.
- [11] Casacci, S., Gentilini, C., Di Tommaso, A., Oliveira, D.V. Shear strengthening of masonry wallettes resorting to structural repointing and FRCM composites. *Construction and Building Materials* (2019) 206: 19-34.

- [12] Ceroni, F., Maddaloni G., Pecce M. Pull-out tests on injected anchors in tuff masonry elements. *Key Engineering Materials* (2017) 747: 326-333.
- [13] Carozzi, F.G., Colombi, P., Fava, G., Poggi, C. Mechanical and bond properties of FRP anchor spikes in concrete and masonry blocks. *Composite Structures* (2018) 183: 185-198.
- [14] Castori, G., Borri, A., Corradi, M., Righetti, L. Structural analysis of transversal steel connectors applied on multi-leaf walls. In 13th Canadian Masonry Symposium, Halifax, Canada, (2017).
- [15] Silveri, F., Riva, P., Profeta, G., Poverello, E., Algeri C. Injected anchors for the seismic retrofit of historical masonry buildings: experimental study on brick masonry. In International Conference Proceedings of SAHC2014 – 9th International Conference on Structural Analysis of Historical Constructions, F. Peña & M. Chávez (eds.), Mexico City, Mexico (2014).
- [16] Cascardi, A., Leone, M., Aiello, M.A. Shear behavior of multi leafs masonry panels with transversal connections. *Key Engineering Materials* (2019) 817: 359-364.
- [17] Corradi M., Borri A., Poverello E., Castori G. The use of transverse connectors as reinforcement of multi-leaf walls. *Materials and Structures* (2017) 50: 114.
- [18] Moreira, S., Ramos, L.F., Csikai, B., Bastos, P. Bond behavior of twisted stainless steel bars in mortar joints. In International Conference Proceedings on 9th International Masonry Conference, Guimarães (2014).
- [19] Donnini, J., Maracchini, G., Chiappini, G., Corinaldesi, V., Quagliarini, E., Lenci, S. Can Textile Reinforced Mortar (TRM) systems be really effective to increase compressive strength of masonry panels? *Key Engineering Materials* (2019) 817: 435-441.
- [20] Chen P., Finelli F., Franzoni E., Gentilini, C., Sansone, G. Preliminary experimental results on the pull-out behavior of twisted steel connectors in masonry units of different materials. *Key Engineering Materials* (2019) 817: 371-376.
- [21] Finelli, F., Di Tommaso, A., Gentilini C. First results of a 3D pull-out model of steel anchors in fired-clay bricks. *Key Engineering Materials* (2019) 817: 514-519.
- [22] Girelli, V.A., Tini, M.A., Dellapasqua, M., Bitelli, G. High resolution 3D acquisition and modelling in cultural heritage knowledge and restoration projects: The survey of the fountain of Neptune in Bologna. In *Int. Arch. Photogramm. Remote Sens. Spatial Inf. Sci.*, XLII-2/W11, (2019): pp. 573–578.
- [23] Castellazzi, G., D’Altri, A.M., Bitelli, G., Selvaggi, I., Lambertini, A. From laser scanning to finite element analysis of complex buildings by using a semi-automatic procedure. *Sensors* (2015) 15: 18360-18380.

- [24] Sansoni, G., Trebeschi, M., Docchio, F. State-of-the-art and applications of 3D imaging sensors in industry, cultural heritage, medicine, and criminal investigation. *Sensors* (2009) 9: 568–601.
- [25] Bitelli, G., Simone, A., Girardi, F., Lantieri, C. Laser scanning on road pavements: a new approach for characterizing surface texture. *Sensors* (2012) 12: 9110-9128.
- [26] Laghi, V., Palermo, M., Gasparini, G., Girelli, V.A., Trombetti, T. Experimental results for structural design of Wire-and-Arc Additive Manufactured stainless steel members. *Journal of Constructional Steel Research* (2019):105858.
- [27] Francolini, C., Marchesi, G., Bitelli, G. High-resolution 3D survey and visualization of Mesopotamian artefacts bearing cuneiform inscriptions. In 2018 IEEE International Conference on Metrology for Archaeology and Cultural Heritage, Danvers (MA), Institute of Electrical and Electronics Engineers, (2018).
- [28] Sandrolini, F., Franzoni, E., Cuppini, G., Caggiati, L. Materials decay and environmental attack in the Pio Palace at Carpi: a holistic approach for historical architectural surfaces conservation. *Building Environment* (2007) 42: 966– 1974.
- [29] Colella A., Di Benedetto C., Calcaterra D., Cappelletti P., D'Amore M., Di Martire D., Graziano S.F., Papa L., de Gennaro M., Langella A. The Neapolitan yellow tuff: An outstanding example of heterogeneity. *Construction and Building Materials* (2017) 136: 361-373.
- [30] Calia, A., Laurenzi Tabasso, M., Mecchi, A.M., Quarta, G. The study of stone for conservation purposes: Lecce stone (southern Italy). *Geological Society* (2014), London, Special Publications, 391: 139-156.
- [31] Maragna, M., Gentilini, C., Castellazzi, G., Carloni, C. Bond of steel bars to masonry mortar joints: Test results and analytical modelling. *Key Engineering Materials* (2017) 747: 319-325.
- [32] EN 772–1 "Methods of test for masonry units - Part 1: Determination of compressive strength".
- [33] EN 14580 "Natural stone test methods. Determination of static elastic modulus".
- [34] EN 12390-6 "Testing hardened concrete. Tensile splitting strength of test specimens".
- [35] Santandrea, M. Bond behavior between fiber reinforced composites and quasi-brittle material interfaces, University of Bologna, Ph.D. Dissertation Thesis, Ph.D. program in Civil, Chemical, Environmental and Materials Engineering, (2018).

- [36] Sandrolini, F., Franzoni, E., Cuppini, G. Predictive diagnostics for decayed ashlar substitution in architectural restoration in Malta. *Materials Engineering* (2000) 11: 323–337.
- [37] Technical data sheet of ‘Steel DryFix®’:  
[http://products.kerakoll.com/gestione/immagini/prodotti/Steel%20DryFix%2010%20ITA\\_rating%202019.pdf](http://products.kerakoll.com/gestione/immagini/prodotti/Steel%20DryFix%2010%20ITA_rating%202019.pdf)
- [38] Zezza, U., Veniale, F., Zezza, F., Moggi, G. Effetti dell'imbibizione sul decadimento meccanico della pietra leccese. In *Proceedings of the 1st Int. Symp. on The Conservation of Monuments in the Mediterranean Basin*, Bari 1989: 263-269.